Powder Metal Main Bearing Cap Durability and Fatigue Analysis using Density-Distribution-Based Mechanical Properties

Mohammed Z. Abedin[1], Cherng-Chi Chang[1], Bing Li[1], Y. Hammi[2]

and M. F. Horstmeyer[2]

[1]General Motors (GM), [2]Mississippi State University (MSU)

Abstract: Durability analysis of a powder metal (PM) automotive engine component main bearing cap (MBC) is typically performed assuming uniform material properties. However, the mechanical properties of powder metal components vary significantly with density. Mississippi State University (MSU) developed mathematical-based user material subroutines VUMAT and UMAT in Abaqus to model the compaction and sintering processes of powder metal components (Hammi et al., 2010). This model can predict the distribution of material density during PM compaction analysis in Abaqus/Explicit. In this paper, based on the density distribution from compaction analysis of a PM main bearing cap, material properties are mapped onto the PM cap for durability stress analysis in Abaqus/Standard under typical automotive engine operating conditions. Density distribution-based fatigue material properties are interpolated/ extrapolated using PM main bearing cap density distribution and experimental fatigue life curves at two different densities (high and low). High-cycle fatigue evaluation of the PM main bearing cap is then performed with the fatigue code fe-safe using non-uniform fatigue material properties along with stress results from durability analysis, which also uses non-uniform mechanical properties. These high-cycle fatigue results are compared with the fatigue results of main bearing cap analysis using uniform material properties.

Keywords: Powder Metal, Density Distribution, Compaction, Durability, High-Cycle Fatigue, Finite Elements, Powertrain.

1. Introduction

An increasing number of automotive components are being converted to PM technology. In order to properly engineer these components, it is necessary to understand the material and processing methods to obtain the appropriate mechanical behavior appropriate for the application. Accurate modeling of material behavior is vital for accurate prediction of the performance of structural components. A project was initiated and supported by USCAR to develop math-based predictive tools with test validation to accurately describe properties of non-forged powder metallurgy components in order to reduce design time and development costs and aid in optimizing component performance. The Center for Advanced Vehicular Systems (CAVS) of Mississippi State University carried out the project successfully by developing a math-based material model in

Abaqus/Explicit and Abaqus/Standard to predict density distribution during the PM manufacturing process and validating this model with test data (Hammi et al., 2010). This math-based PM material model was applied and the analysis procedure was further developed in an automotive engine PM component such as a main bearing caps (MBC) under engine operating conditions to predict high-cycle fatigue performance.

2. Die Compaction

2.1 Compaction constitutive model

Die compaction is the first consolidation process of the PM press-sinter process. Here, a modified Drucker-Prager/Cap material model originally proposed by DiMaggio and Sandler (1971) for soils mechanics (Figure 1) is used to model the powder behavior during densification. The plastic flow is defined by two dissipation potentials that are respectively non-associated to the failure envelope F^e in the low pressure region, and associated to the cap yield surface F^c in the high pressure region:

$$F^e = |s - \alpha| - \kappa - d - p \tan\beta - f_t(p, p_a) = 0, \quad (1)$$

where β is the material's angle of friction and d is its cohesion strength, both are function of the relative density ρ (Coube and Riedel, 2000). The failure yield surface is smoothly connected to the cap yield surface using a transition function f_t in the failure yield surface F_s. The cap hardening variable p_a is an evolution parameter that represents the volumetric plastic strain-driven hardening/softening (Figure 1). At high densities (near fully dense material), the powder aggregate is described by a Mises type yield surface with isotropic hardening κ and kinematic hardening $\underline{\alpha}$. Therefore, for the stress state $p \geq p_a$, the cap surface is replaced by a Mises yield surface (Figure 1).

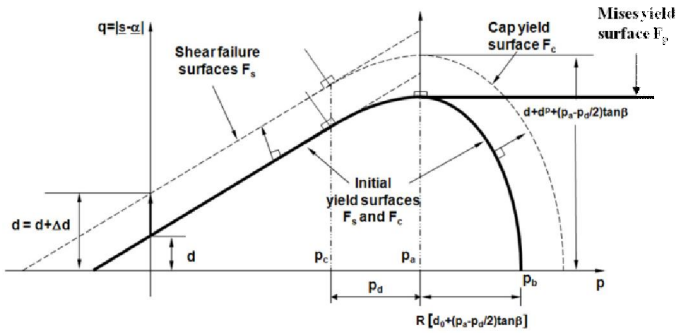

Figure 1. Modified Drucker-Prager/Cap Model: yield surfaces in the (q–p) plane.

The cap yield surface F^c has an elliptical shape in the meridional (q–p) plane and is written as

$$F^c = \sqrt{|s - \alpha|^2 - \frac{1}{R^2}[p - p_a]^2} - F_e(d, p_a) = 0, \quad (2)$$

where $R=R(\rho)$ is the cap eccentricity that controls the shape of the cap. The evolution parameter p_a is also defined as a hardening parameter that controls the motion of the cap surface, and p_b defines the geometry of the cap surface. The ellipticity of the cap surface is determined by the material eccentricity parameter R that relates the hardening parameter p_a to p_b through the relation:

$$p_b = p_a + RF^e(p_a) \tag{3}$$

Sandler and Rubin (1979) proposed a relationship to define the evolution of the cap's motion, which is defined by the isotropic cap hardening rule

$$\bar{\varepsilon}_{vol}^{p} = W\left(1 - \exp\left[-c_1(p_b - p_{b|_0})^{c_2}\right]\right) \tag{4}$$

where p_b the hydrostatic compression yield stress, $\bar{\varepsilon}_{vol}^{p}$ is the effective volumetric plastic strain, W is the maximum plastic volumetric strain (at hydrostatic compression *'lockup'*), c_1 and c_2 are material parameters, and $p_{b|0}$ is the initial value of p_b.

2.2 Powder Characterization

A number of experimental tests and density measurements on an FC-0208 powder with 0.6% Acrawax have been performed to gather the data necessary for characterization and validation of the constitutive equations of compaction and sintering. Brazilian, compression and compressibility tests on cylindrical green samples were used to determine the failure line and cap surface at different densities (Coube and Riedel, 2000).

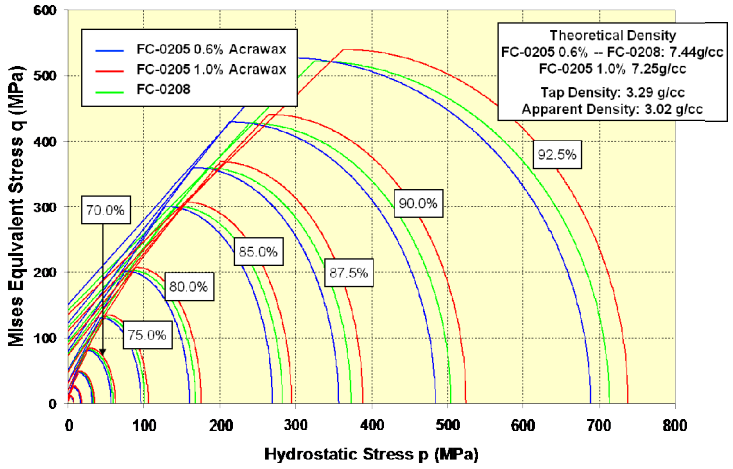

Figure 2. Isodensity curves in the p-q plane for FC-0205 and FC-0208 powders.

The resonant frequency method was applied to green compacts of different densities to determine the evolution of elastic properties during compaction. Figure 2 shows the equidensity lines in the *(p–q)* stress space, which correspond to the evolution of the Modified Drucker/Prager compaction

model during densification.

2.3 Die Compaction of Main Bearing Cap

Using the Modified Drucker/Prager constitutive model for powder compaction, implemented in the user material subroutine VUMAT of Abaqus/Explicit, FE numerical analyses of a closed-die compaction of a MBC were performed (Hammi et al., 2010). All dies and punches were assumed rigid, meshed with R3D4 elements, and moving tools were prescribed velocities as boundary conditions. The density before compaction was initialized with a non-uniform distribution to account of the density gradient caused by the die wall friction during die filling. Wikman et al. (2000) estimated the coefficient of friction by combining an experiment with modeling of the experiment. They evaluated that the die-wall friction coefficient ranges from about 0.2 at high densities to 0.8 or even higher at low densities. In this calculation, the die-wall friction was given a constant value of μ=0.2, corresponding to friction conditions for a very high punch force. Figure 3 shows the density distribution of the compacted MBC in the die and before ejection for the FC-0208 powder along with a curve showing change of density during compaction at a particular node location.

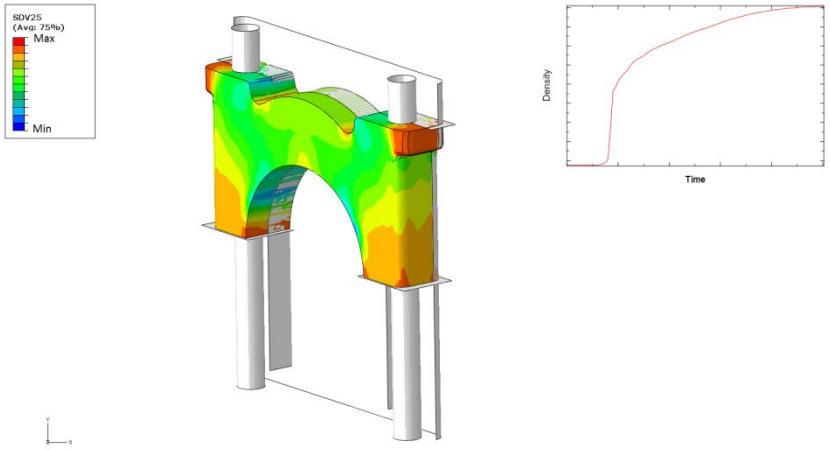

Figure 3. FEA simulation showing the MBC green density distribution at the end of compaction (in the die) for a FC-0208 0.6% Acrawax material and nodal density history.

The ejection phase was simply performed by a spring-back analysis in Abaqus/Standard, in which the MBC geometry and model were imported from Abaqus/Explicit. During this spring-back simulation, no further powder densification was considered, and the powder compact behavior was assumed elastic. The Young's modulus was defined as a function of the green relative density ρ. During spring-back, the volume grew about 0.6% and dominant dimensional changes occurred along the compacting direction as shown in Figure 4.

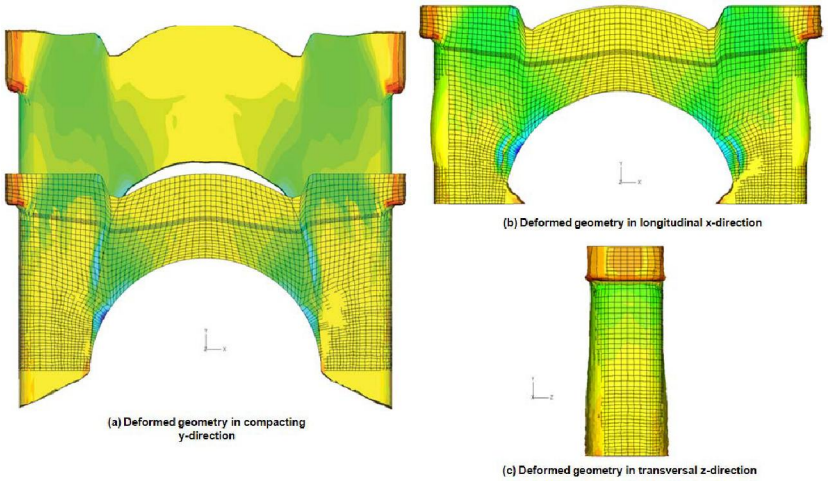

Figure 4. Geometry of MBC before spring-back (with mesh) and after spring-back (without mesh) with a deformation scale factor of 100.

3. Powder Metal (PM) Main Bearing Cap (MBC) Durability Analysis

3.1 PM MBC Durability Model

The main bearing cap (MBC) supports the main bearings of the crankshaft in an automotive engine. With increased horsepower and torque requirements in automotive industry, the durability of the main bearing caps is essential to a robust engine design, and accurate analytical modeling is one of the key enablers. In this study, a bulkhead "slice" FEA assembly model of a six cylinder in-line automotive engine was used to simulate durability analysis of a PM MBC under engine operating conditions in Abaqus/Standard. Figure 5 shows the MBC model in the engine slice assembly.

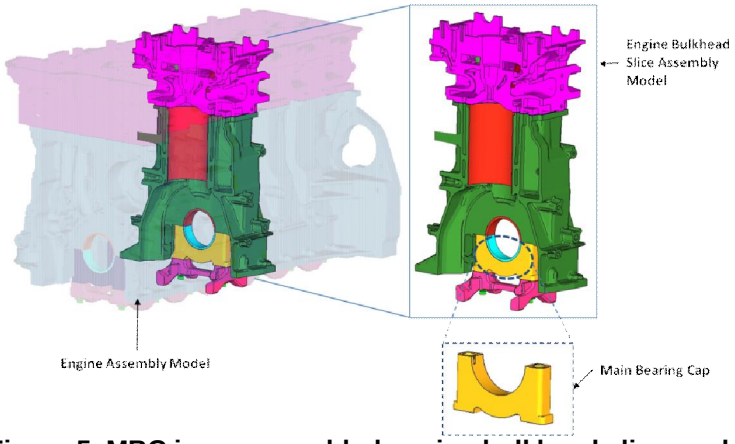

Figure 5. MBC in an assembled engine bulkhead slice model.

The PM MBC durability model was meshed using C3D10 elements in the engine assembly slice. The density distribution was mapped using the feature *MAP SOLUTION in Abaqus/Standard from the PM compaction process analysis, or more precisely, from the spring-back analysis. Figure 6 shows the density distribution of the PM MBC after spring-back as well as density distribution after mapping on the MBC durability model.

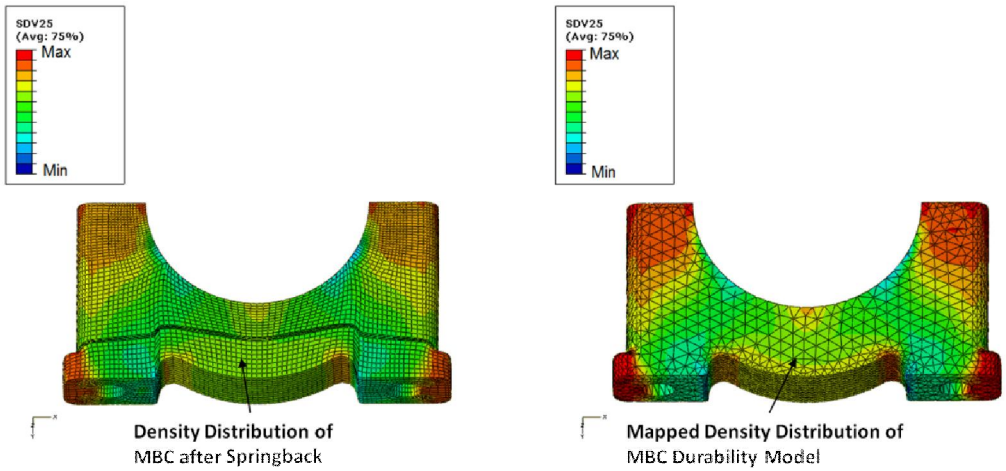

Figure 6. Density distribution contours of the spring-back and durability models.

The Young's modulus at each material point of the MBC was calculated within a material subroutine UMAT as a function of the porosity ø according to:

$$E(ø) = E_0 (1 - ø)^{\beta} \tag{5}$$

where E_0 is the Young's modulus of the raw material and β a shape parameter. The density distribution-based calculated elemental Young's distribution on the MBC durability model is shown in Figure 7.

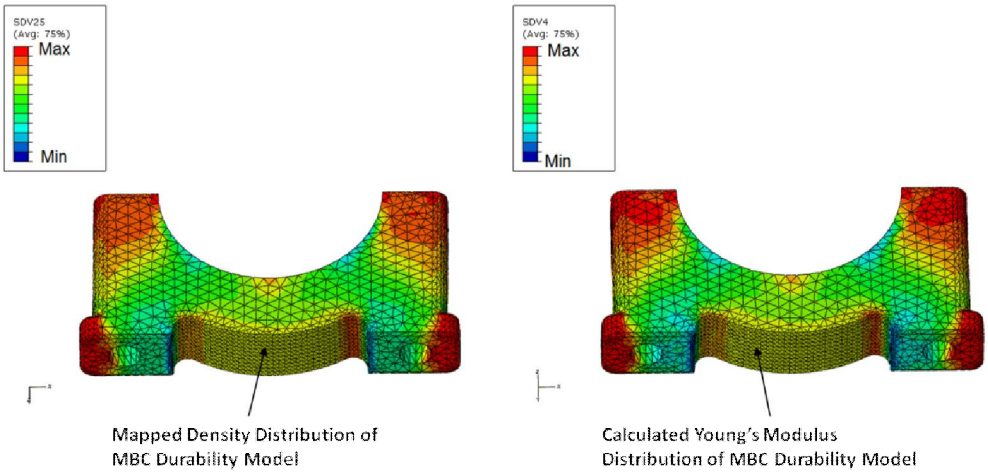

Figure 7. Density and Young's modulus distribution contours of a MBC durability model.

3.2 PM MBC Durability Stress Analysis in Abaqus/Standard

Durability analysis of a PM main bearing cap assembled in engine bulkhead slice model was done in Abaqus/Standard using a non-uniform elemental Young's modulus under engine operating conditions at 6200rpm. Linear uniform material properties were assigned for other components in the assembly listed in Table 1.

Table 1. Material properties used for different components in the engine bulkhead slice model.

Component	Material	Density Mg/mm3	Young's Modulus MPa	Poisson's Ratio
Head, Block	Aluminum	2.72E-09	72000	0.32
Liner	Iron	7.3e-09	93000	0.28
Valve Seat	Seats	7.0e-09	120000	0.24
Valve Guide	Guides	7.0e-09	80000	0.23
Bearing Shell	Steel	7.8e-09	210000	0.3
Bolts	Steel	7.8e-09	210000	0.3
PM MBC	FC-0208	Mapped	Calculated Non-Uniform	0.28

Non-linear gasket loading/unloading curves were specified using GK3D# elements for the multi-layer steel (MLS) cylinder head gasket. Interface contacts were defined between mating surfaces, assigning a friction coefficient for small sliding contact. Press-fits were assigned between block

and liner. The loads considered for the engine bulkhead slice durability analysis under the engine operating conditions of interest are listed in Table 2.

Table 2. Abaqus/Standard load steps for engine bulkhead slice durability analysis.

Assembly Load	Head Bolt Pre-Load
	Main Bearing Bolt Pre-Load
Thermal Load	Assumed Thermal Load
Combustion Load	Cylinder Pressure @ 6200rpm
	Piston Side Loads @6200rpm
	Main Bearing Loads @6200rpm

The combustion loads are shown in Figure 8 for main bearing loads, cylinder chamber pressure and piston side loads.

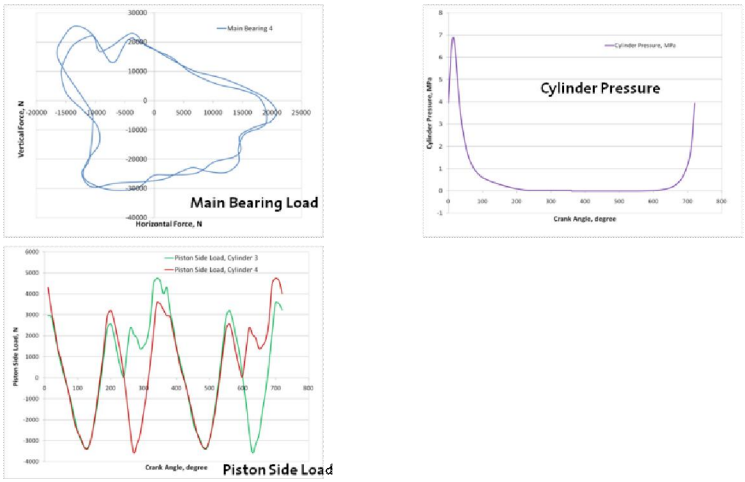

Figure 8. Combustion loads applied in engine bulkhead slice durability analysis.

Elemental material properties of the MBC were used as *INTIAL CONDITION, TYPE=SOLUTION in Abaqus/Standard. A user subroutine UMAT was used to calculate stress tensors of the MBC based on elemental material properties in the Abaqus/Standard durability analysis. The nodal stress tensor histories of the PM MBC from durability analysis were used to calculate high-cycle fatigue performance.

4. PM MBC High-cycle Fatigue Analysis

4.1 PM MBC Non-Uniform Fatigue Material Properties

A PM MBC has a non-uniform density distribution after compaction as shown in Figure 6. CAVS conducted fatigue tests of MBC samples at room temperature for two different densities – high and low. Lower and upper bounds of fatigue life were determined from the strain-controlled low-cycle fatigue tests on samples of respective low and high densities (Figure 9). The fatigue

parameters were then calibrated on the low-cycle fatigue curve, and extrapolation for the high-cycle regime was performed using the MSFfit software developed at CAVS.

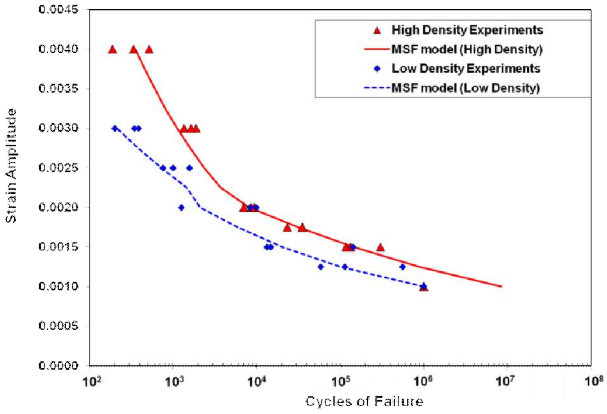

Figure 9. Strain amplitude vs. cycle-to-failure curve for bounds of lower and higher densities.

Based on the room temperature fatigue test data provided by CAVS at lower and upper densities of PM MBC samples shown in Figure 9, cyclic fatigue coefficients and exponents were calculated, which were needed to calculate Neuber-corrected high-cycle fatigue safety factors of the PM MBC durability model. These coefficients and exponents are listed in Table 3 (Sl. Nos. 6 to 9) for two different densities.

The cyclic fatigue properties of PM MBC listed in Table 3 for two densities, low and high, were used to calculate the cyclic fatigue properties for the whole PM MBC durability model based on density distribution as shown in Figure 6. An interpolation/extrapolation code was developed to perform this calculation. Figure 10 shows the calculated high-cycle fatigue strength (HCFS) distribution and ultimate tensile strength (UTS) distribution of the PM MBC based on density distribution of the PM MBC durability model.

Table 3. Low- and high-density PM FC-0208 fatigue material properties.

Sl. No.	PM FC-0208	1 - Low Density	2- High Density
1	Density, g/cc	6.32	6.94
2	E, MPa	123000	168000
3	UTS, MPa	431	503
4	HCFS (1e7 cycles), MPa	81.9	138.5
5	LCFS (1e4 cycles), MPa	172.6	290
6	Cyclic Strength Coeff. K´, MPa	7926.7	3466.5
7	Cyclic Strength Exponent, n'	0.4882	0.3159
8	Fatigue Strength Coeff. σ'_f	502.99	836.82
9	Fatigue Strength Exponent, b	-0.108	-0.107

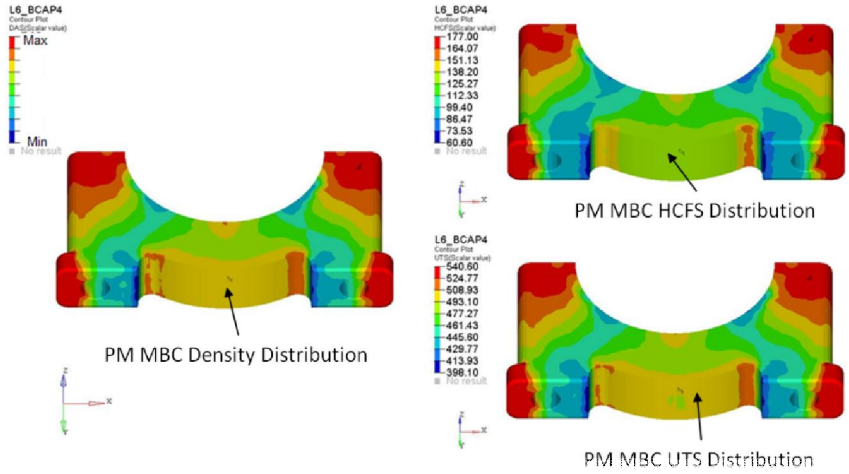

Figure 10. Density and fatigue properties distribution contour plots of a PM MBC.

4.2 PM MBC High-Cycle Fatigue Calculations in fe-safe

High-cycle (10^7) fatigue evaluation of PM Main Bearing Cap was done using the commercial fatigue code fe-safe. The nodal stress tensor histories of the MBC from Abaqus/Standard FEA durability analysis were imported into fe-safe. The calculated non-uniform nodal fatigue material property distributions were imported into fe-safe using a utility macro. The critical plane-based principal stress method was used for fatigue calculation of a PM MBC in fe-safe. A user-defined mean stress correction was used to calculate the Fatigue Reserve Factor (FRF, also called Fatigue Safety Factor) for high-cycle fatigue evaluation. The high-cycle fatigue results of a PM MBC using non-uniform material properties (NUP) were compared with the high-cycle fatigue results of a MBC using uniform material properties for the following three cases:

A. MBC durability and fatigue analysis using High-Density Uniform Properties (HDUP)
B. MBC durability and fatigue analysis using Low Density Uniform Properties (LDUP)
C. MBC durability and fatigue analysis using Average Density Uniform Properties (ADUP)

Mechanical and fatigue properties used for the above three cases are listed in Table 4.

Table 4. PM FC-0208 material properties, three different uniform densities.

PM FC-0208	A - High Density	B - Low Density	C - Ave. Density
Density, g/cc	6.94	6.32	6.63
E, MPa	168000	123000	145500
UTS, MPa	503	431	467
HCFS (1e7 cycles), MPa	138.5	81.9	110.2
Cyclic Strength Coeff. K´, MPa	3466.5	7926.7	5696.6
Cyclic Strength Exponent, n'	0.3159	0.4882	0.4021
Fatigue Strength Coeff. σ'_f	836.82	502.99	669.91
Fatigue Strength Exponent, b	-0.107	-0.108	-0.108

The high-cycle safety factor contour plots of a MBC are shown in Figure 11, where two particular low safety factor locations of a MBC using non-uniform properties are compared with the safety factors at the same locations in three other cases using uniform material properties. The predicted lowest safety factor based on non-uniform properties (location A shown in Figure 11) was below the durability design target, and its location matched well with the crack initiation location (Figure 12) found at the end of a fatigue test. The crack in a failed bearing cap after a fatigue test typically starts at the location shown by the arrow in Figure 12 and continues toward the arch of the inner diameter. Most of the failures did not show a complete fracture through the arch. In most of the tests, a crack 1/8"–1/4" long was observed on both lateral sides of the cap after the test had completed 10^7 cycles (Ilia et al., 2003).

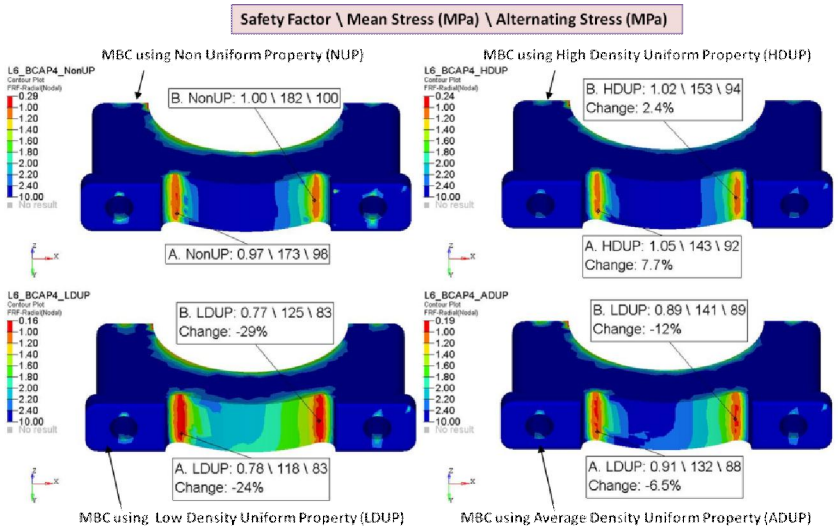

Figure 11. High-cycle (10^7) safety factor contour plots of a MBC with non-uniform and three different uniform material property assumptions.

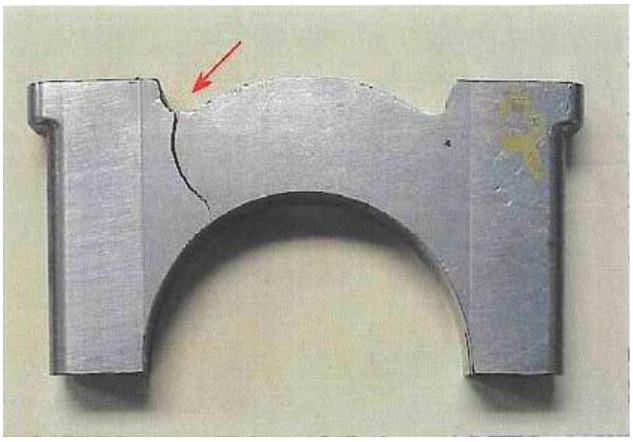

Figure 12. Typical fatigue failure in a PM MBC (Ilia et al., 2003).

Locations A & B shown in Figure 11 are near bolt holes as well as in geometric transition areas. Both of these locations are highly stressed by both mean stresses from assembly and thermal loads as well as alternating stress from combustion loads.

The results shown in Figure 11 and listed in Table 5 compare the high-cycle fatigue safety factors at locations A&B due to the different density assumptions, described above. The results for the MBC with high-density uniform properties (HDUP) predicted higher safety factors than those using non-uniform properties (NUP) for locations A & B by 7% and 2% respectively, which could be overly-optimistic for fatigue evaluation. On the other hand, the results for the MBC using low-density uniform properties (LDUP) and average-density uniform properties (ADUP) predicted lower high-cycle safety factors in both locations compared to the safety factors in the same locations for a MBC using the NUP approach.

Out of these four cases, LDUP predicted up to 29% lower fatigue performance of a MBC, and ADUP showed up to 12% lower safety factors. Both LDUP and ADUP approaches could be too conservative in MBC durability analysis compared to the NUP approach.

Table 5. Comparison of MBC high-cycle fatigue results.

MBC Model	Location	Safety Factor	Mean Stress, MPa	Alternating Stress, MPa	% Change In Safety Factor
NUP	**A**	0.97	173	98	
HDUP	**A**	1.05	143	92	7.7
LDUP	**A**	0.78	118	83	-24.2
ADUP	**A**	0.91	132	88	-6.5
NUP	**B**	1.00	182	100	
HDUP	**B**	1.02	153	94	2.4
LDUP	**B**	0.77	125	83	-29.4
ADUP	**B**	0.89	141	89	-11.9

5. Conclusion

An analysis technique was presented in this paper where density-based mechanical and fatigue material properties were used for powder metal main bearing cap durability design analysis under automotive engine operating conditions. The density distribution was predicted from powder metal compaction analysis using the MSU CAVS-developed and -validated material constitutive model, which was utilized to calculate non-uniform mechanical properties of the PM MBC for durability stress analysis. This density distribution was also used to calculate non-uniform fatigue material properties of a PM MBC, which were implemented to predict high-cycle fatigue performance of a MBC using the fatigue code fe-safe. High-cycle fatigue evaluation of a PM MBC using these density-based non-uniform material properties showed good correlation of the lowest safety factor location with the crack location of a MBC after fatigue testing. At the same time this analysis technique provides a more accurate prediction tool for high-cycle fatigue performance of a MBC compared to the optimistic prediction using high-density material property, as well as compared to the conservative prediction of the same using low-density and average-density material properties.

6. Acknowledgment

The authors would like to acknowledge guidance from the Center for Powder Metal Technology (CPMT) on the development and validation of the powder metallurgy constitutive model, as well as on the application of this model to durability analysis. We also acknowledge guidance from Jayaraman Sivakumar (GM), Jennifer Cook (GM) and Shekhar Wakade (GM).

7. References

1. Abaqus, User's Manual, Version 6.7, ABAQUS Inc., 2007.
2. Coube, O. and H. Riedel, "Numerical Simulation of Metal Powder Die Compaction with Special Consideration of Cracking," Powder Metallurgy, 2000, Vol. 43, No. 2, pp. 123–131.
3. DiMaggio, F.L. and I.S. Sandler, "Material Models for Granular Soils," Journal of Engineering Mechanics, ASCE, 1971, Vol. 97, EM3, pp. 935–950.
4. Fe-safe User Manual, Version 5.4-04, Safe Technology Limited, 2008.
5. Hammi, Y., T.W. Stone, P.G. Allison, and M. F. Horstemeyer, "Fatigue Modeling of a Powder Metallurgy Main Bearing Cap," SIMULIA Customer Conference, 2010.
6. Ilia, E., M. O'Neill, J. Lee, J. Poirier, and S. St-Laurent, "Development of a Main Bearing Cap for an Inline 6 Cylinder Engine," Advances in Powder Metallurgy and Particulate Materials, Part 9, pp. 9-22–9-35, 2003.
7. Sandler, I.S., and D. Rubin, "An Algorithm and a Modular Subroutine for the Cap Model," International Journal for Numerical and Analytical Methods in Geomechanics, Vol. 3, pp.173–186, 1979.
8. Wikman, B., N. Solimannezhad, R. Larsson, M. Oldenburg, and H.-A. Haggblad, "Wall friction coefficient estimation through modelling of powder die pressing experiment," Powder Metallurgy, Vol. 43, No. 2, pp. 132–138, 2000.